PCCP

RSC Publishing

PAPER

View Article Online
View Journal | View Issue

Cite this: *Phys. Chem. Chem. Phys.*, 2013, **15**, 19879

A liquid CO_2-compatible hydrocarbon surfactant: experiment and modelling

Soumi Banerjee,* J. Mieke Kleijn, Martien A. Cohen Stuart and Frans A. M. Leermakers

Received 20th June 2013,
Accepted 24th September 2013

DOI: 10.1039/c3cp52571f

www.rsc.org/pccp

Surfactants soluble in liquid CO_2 are rare and knowledge on interfacial and self-assembly behaviour is fragmented. We found that polyoxyethylene (5) isooctylphenyl ether is interfacially active at the water–liquid CO_2 interface. Water–liquid CO_2 interfacial tension was measured at various surfactant concentrations at 50 bar and 283 K using the pendant drop method, and a CMC like cusp was observed at a surfactant concentration of $\sim$50 mM in the bulk liquid CO_2. This system was modelled applying the self-consistent field theory of Scheutjens and Fleer (SF-SCF). We use a free-volume approach, wherein the chemical potential of the vacancies was linked to the pressure and the molecules were described using a freely-jointed chain model on a united atom level. The model indicates that typically the water–vapour interface is wet by CO_2. Interestingly, a window of partial wetting was identified at the water–vapour interface as a function of the chemical potential of the surfactant. The second-order nature of both wetting transitions is attributed to the close proximity to the critical point of the CO_2–vapour system. Furthermore, the SF-SCF theory was used to study the self-assembly of the surfactant in bulk CO_2 or water, focusing on the three-phase coexistence, that is at P/P_{sat} = 1. Above $\sim$40 mM in the CO_2-rich phase, the theory indicates stable water swollen reverse micelles with an aggregation number of $\sim$100. The analysis further shows the stability of compressible CO_2-swollen surfactant bilayers in the bulk water phase at elevated surfactant concentrations. Finally it was found that the critical reverse micellar concentration (in liquid CO_2) increases and the aggregation number decreases with increasing pressure.

1 Introduction

The phase behaviour of surfactants in biphasic solvent systems is of interest for both academia and industry. For example, in oil–water systems surfactants, which are inherently both lyophilic and lyophobic (HLB $\sim$ 10), can partition in both solvents and then form a rich variety of mesophases, which pose challenging modelling problems. Although oil–water systems containing amphiphiles are often encountered in practice in the form of emulsions and microemulsions, systematic theoretical investigation of these systems is scarce.[1,2] Compared to the formation of micelles in water, the reverse micellization of surfactants in apolar media has been relatively less studied in particular when water is also present in such systems as a second phase.

In this paper, we consider biphasic liquid CO_2–water systems in the presence of a CO_2 soluble surfactant. Hydrocarbon surfactants, soluble in liquid CO_2, are encountered rarely. For those that exist, understanding their phase behaviour in liquid CO_2 is either lacking or superficial. The ongoing challenge to find soluble amphiphiles for liquid CO_2 is hampered by the lack of specialised high pressure equipment needed for this search. Liquid CO_2 appears to be a poor solvent for most hydrocarbon surfactants, as it is unable to screen the tail–tail attractions between the surfactants. These aspects have been discussed in detail in ref. 3 and 4.

Computer simulations have been used to model surfactant phase behaviour in supercritical (sc) CO_2, sc CO_2–water or sc CO_2–water–alcohol mixtures using the coarse grained lattice Monte Carlo approach of Larson[5] or a slightly modified version[6] thereof. In some cases models covering atomistic details were also employed, *e.g.*, for the self-assembly in double chain surfactant–sc CO_2–water ternary systems.[7–9] In our study we focus on a hydrocarbon amphiphile with methyl branching in the apolar tail. Such surfactants have previously been identified as suitable for liquid CO_2, following the argument of fractional free volume.[3,4] In our previous publication we have introduced polyoxyethylene (5) isooctylphenyl ether (Igepal CA 520) as a potential surfactant for liquid CO_2 from the perspective of dry-cleaning.[4] In the present paper we first present the experimental interfacial tension of this hydrocarbon surfactant at the water–liquid CO_2 interface.

Laboratory of Physical Chemistry and Colloid Science, Wageningen University, Dreijenplein 6, 6703 HB Wageningen, The Netherlands.
E-mail: soumi.banerjee@wur.nl

We then employ the lattice based self-consistent field of the Scheutjens and Fleer (SF-SCF) model targeted to enhance our molecular understanding (surface phase behaviour of liquid CO_2 in the presence of the surfactant, micellar shape, size, aggregation number, bilayer formation) of the various self-assembled structures formed by this surfactant in the biphasic system, water–liquid CO_2. This may seem to be a gigantic effort, but the SF-SCF is so efficient that it turned out possible to scan a large phase and parameter space in very short time allowing us to develop an appropriate model and a parameter set to first order.

This paper is a follow up of two of our previous studies, namely ref. 10 where we introduced self-consistent field modelling to predict the properties of the CO_2–water interface and ref. 4 where we have shown experimentally the effectiveness of Igepal CA520 towards particle release in liquid CO_2. In this paper, we build upon the SF-SCF model that we have used in ref. 10 by incorporating the surfactant as an additional molecular component. The paper is organized as follows: we first briefly discuss experimental and theoretical aspects. This is followed by a more extensive discussion of parameter values in the model. While discussing the self-consistent field theory we refer to our previous publication,[10] where we already discussed the scheme in general. Moreover, the interaction parameters between the segments of water, free volume and CO_2 were already introduced in ref. 10. Hence, in the present paper we focus on the self-consistent field treatment of chain like molecules. Most of the extra modelling parameters we deduce from previous studies.[11] However, some of the parameters, typically those involving the CO_2 molecule are unknown and we here will give a suggestion for appropriate values. In the Results and discussion section we perform a short parameter survey. From this study we obtain insights into why the micellisation of surfactants in liquid CO_2 is so difficult.

We then characterize the adsorption of surfactants at the water–vapour interface by measuring the corresponding interfacial tension. The modelling of this leads us to consider the wetting behaviour of CO_2 at this surfactant-decorated interface. More specifically, we show how the presence of a surfactant at the water–vapour interface may influence the wetting of this interface by liquid CO_2.

Next we employ the self-consistent field theory to study the self-assembly of the surfactant in the bulk CO_2 or the water phase. We explore the nature of the assemblies, and the sequence in which they occur as the chemical potential of the surfactant is gradually increased.

2 Materials and methods

The interfacial tension between deionized water and liquid CO_2 (Westfalen Gas, purity 99.5%) in the presence of Igepal CA520 (Sigma Aldrich, purity >99%, molecular weight 427 g mol^{-1}) was measured using the pendant drop technique in a high pressure view cell equipped with two transparent windows.[12] The surfactant concentration in liquid CO_2 was varied between 0 and 12% (v/v). The cell volume was $\sim$30 ml.

The cell was filled with liquid CO_2 and a water drop was generated at the end of a steel capillary. A CCD camera recorded the image of the drop, the shape of which was then analyzed using the DSA software (Kruss, GmbH). Details of the pendant drop technique can be found in ref. 13 and 14.

The experimental and modelling results were presented as a function of P/P_{sat}. The interfacial tensions (IFTs) were measured at 50 bar and 283 K and $P/P_{sat} \approx 1.2$ (P_{sat} = 44.5 bar at 283 K). The IFT calculations in the model correspond to P/P_{sat} of $\sim$1.2. For the study of self-assembly in CO_2 and/or water we focused on the three phase co-existence, *i.e.* at $P/P_{sat} = 1$. We also predicted the effect of pressure on the thermodynamics of reverse micellization using the SF-SCF theory and for that we varied P/P_{sat} between 1 and 1.3.

3 Theory

3.1 Pressure in lattice models

The SF-SCF method is lattice based. As the lattice has a fixed volume, this implies an incompressibility constraint. In such a system the pressure is not defined. In order to deal with pressure variations in a previous paper[10] we implemented a lattice-gas variant in which the 'chemical potential' of the vacancy, species V, referring to unoccupied lattice sites, is interpreted as (minus) the pressure times the volume of a lattice site. Besides these vacancies, the lattice is filled with CO_2 and water molecules. The details of the molecular model are further specified below. In this paper we extend this model and elaborate the same (validated) parameter set.

The SF-SCF method is based on similar pre-averaging approximations to the regular solution theory of Flory. This implies that it uses the Bragg–Williams mean-field approximation to evaluate the number of unlike contacts between the monomeric species in the system. The Flory–Huggins interaction parameters were adopted, which take the ''like'' contacts as the reference. For lattice-gas systems it may be more intuitive to take the interactions with the free volume component as the reference. We follow the choices made in our previous paper[10] but note that the reference state is inconsequential for the final results. We specified the conversion rules in our previous paper.

3.2 Chain model

Scheutjens and Fleer originally developed their variant of the SCF theory to model polymer adsorption from solutions.[15] Later, the SF scheme was modified by Leermakers *et al.*[16] to apply the theory to amphiphilic molecules. The conformations of the polymer/amphiphilic chains are evaluated using the freely-jointed chain model (FJC).[15] An obvious concern for FJC models is that a chain can fold back on previously occupied sites. A self-avoiding chain does not have this problem. However, within the SCF approach inter-molecular excluded volume interactions are not rigorously accounted for either. The FJC model accounts for the inter and intra-molecular excluded volume interactions on the same footing. However, a significant advantage of selecting the FJC model is that the single

chain partition function is extremely efficiently computed using the propagator formalism, which gives a huge gain in computation time compared to the algorithm for self-avoiding chains. Moreover, self-avoiding effects are not important for short chains, which are our focus here. We therefore adopt the FJC model. Some details of the lattice used and the propagator formalisms for the surfactant chains are given in the appendix. Below we pay attention to the thermodynamics of self-assembly.

4 Molecular details

As motivated in our previous paper, we chose to model water as a small cluster consisting of five segments (W), in which a central W was surrounded by four neighbours and was represented as W_5. CO_2 was modelled as a dimer (D_2), while the vacancies V occupy just one lattice site. Igepal surfactant molecules are represented by a string of 30 segments as given in Fig. 1a. For comparison the chemical structure of the Igepal CA520 is also shown in Fig. 1b.

In this way we implement that the alkyl-terminus of the surfactant is rich in CH_3 (C3), the central part is rich in CH_2 (C) and the hydrophilic head group is rich in O. The architecture of the surfactant mimics that of the real Igepal, though it is not an exact match *e.g.* the aromatic ring carbons could not fit in the FJC model and therefore we rearrange these segments by putting two of them in the main chain both having two branched segments side by side (Fig. 1a).

5 Interaction parameters

In the self-consistent field theory there are segment potential profiles $u_X(r)$ for each segment type X. Conjugated to these profiles there are computable segment volume fraction profiles $\varphi_X(\mathbf{r})$. The mean field "machinery" may be summarized by

$$\varphi[u(\mathbf{r})] \leftrightarrow u[\varphi(\mathbf{r})] \qquad (1)$$

In words, the SCF algorithm specifies how the volume fraction profiles must be computed from the segment potentials (left hand side of the equation: here the mean field approximation is implemented) and how the potentials follow from the volume fraction profile (right hand side of the equation: here is where the FJC approximation is implemented). The spatial coordinate $\mathbf{r}$ in these functions is the coordinate "perpendicular" to the mean-field directions. For example, for self-assembled bilayers a planar lattice is used wherein the mean field approximation is applied in the x–y planes and the gradient direction is in the z-direction so that $z \equiv \mathbf{r}$. For spherical micelles the gradient direction is in the radial direction and the mean field averaging is over spherical shells of lattice sites. More information about the coordinate systems is given in the appendix.

The short-range attractive and repulsive interactions between various segments of water, CO_2, surfactants and free volume are accounted for by the segment potentials. Each contact (i,j) contributes a (free) energy $\chi_{ij}kT/z$. A positive χ parameter indicates repulsion between unlike segments and a negative value signal attraction. The entropic contributions (translational and conformational entropy) are implemented by the chain model (FJC in our case). Once the fixed point of the equations is reached, usually referred to as the self-consistent solution (*cf.* eqn (1)), it is possible to evaluate the thermodynamic properties of the system. The thermodynamic quantities in turn give information about the feasibility of various options for the self-assembled structures, that is, (reverse) micelles *versus* planar bilayers.

Segments W, D and V already occurred in our previous study of the water–CO_2 system. We retain the parameters that we used there. Here we add new parameters for the segments C, C3 and O. The interaction of these segments with water was taken from previous modelling studies of (nonionic) surfactants in aqueous solutions.[11] The head group oxygen (O) is naturally the most hydrophilic one with $\chi_{WO} = -0.55$ and the tail group segments (C3) are most hydrophobic, having $\chi_{C3W} = 1.55$. The value for χ_{CW} (0.99) was found by fitting CMCs of surfactants in aqueous solutions as a function of the tail length. For more insight, we varied χ_{WO} to see the influence of this parameter on the self-assembly in both water and liquid CO_2. The temperature dependence of non-ionic surfactant assemblies can be implemented by making this parameter temperature dependent, while keeping others constant. Here we take a slightly different approach: we implemented a $1/T$-dependence for all χ parameters. We know from previous studies that we need a significant repulsion between the head and tail segments. This is achieved by taking $\chi_{OC} = 1.77$ and $\chi_{OC3} = 2.21$.

We needed to make educated guesses for the χ parameters between D (the segment of CO_2) and the two different carbon

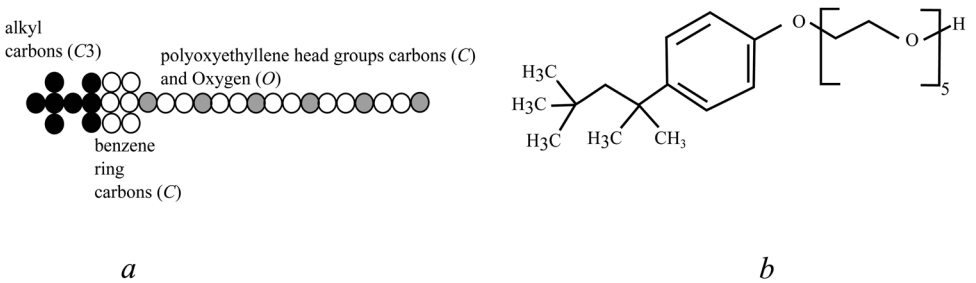

a *b*

Fig. 1 (a) Schematic of the surfactant molecule containing 30 segments each with volume a^3 where a is the length of a lattice site. The black circles, labelled C3, and the white circles, labelled C represent CH_3 and CH_2 groups, respectively. The grey circles represent oxygen or OH (O). (b) Chemical structure of Igepal CA520, branched polyoxyethylene (5) isooctylphenyl ether.

segments and between D and O. One of the arguments that we use is based on the similarity between heptane (modelled as C_7) and CO_2 (modelled as D_2). Heptane has a (small) solubility gap with CO_2.[17] In our model the χ_{DC}^{cr} for the $C_7 - D_2$ system *i.e.* the critical χ parameter below which C_7 and D_2 are still miscible is 0.95 and we assume a slightly higher value of 0.99 between D and C to ensure a solubility gap.[10] The miscibility of the CH_3 (modelled as C3) and D_2 is expected to be significantly better. As a default value we choose $\chi_{C3D} = 0.4$. We vary this parameter to investigate how critical the actual value is for the feasibility of (reverse) micelles in CO_2 and bilayers (in water). Finally, we select a strong repulsion between CO_2 and the oxygen groups of the surfactant, $\chi_{OD} = 1.66$.

From above it is clear that there are several somewhat arbitrary choices for the new parameters. We therefore stress that the validity of the parameters has to be justified *a posteriori*. Moreover, the most critical parameters that affect the micellisation are easily identified and the response to changes in these parameters is presented in the Results and discussion section.

6 Output parameters for surfactant self-assembly

One of the challenges in this study is to quantify the reverse micellization of the surfactant in liquid CO_2. For example, we would like to know when reverse micelles in liquid CO_2 were possibly stable and when these are preferred over liquid crystalline bilayers that might form in the water phase. From quite general considerations and exemplified by the thermodynamics of small systems we know that for thermodynamic stability of association colloids there should be zero excess energy (grand potential) associated with the formation of such objects. That is why we need to compare the chemical potential of the surfactants in the presence of reverse micelles in CO_2 to that in the presence of bilayers in the aqueous phase, under similar conditions. The system with the lowest chemical potential is identified as the most favourable one.

Hence, we need to compute the chemical potentials of the components. Equations exist to evaluate the chemical potential[10] in terms of concentrations of the various components in one of the bulk phases. The SCF method guarantees that in the system there are no chemical potential gradients. We refer to our previous paper for details.[10]

We also require that the grand potential Ω for the association colloids goes to zero. As long as the grand potential $\Omega < 0$ the system tries to create more micelles, and when $\Omega > 0$ the number of micelles will decrease. Only when $\Omega = 0$ an equilibrium situation is obtained.

To consider reverse micelles in bulk CO_2 we select a spherical coordinate system with its origin coinciding with the micellar centre, and lattice layers $r = 1,\ldots,M_r$ where the number of lattice sites, L, grows quadratically, with coordinate r *i.e.*, $L(r) \propto r^2$. The primary result of the SCF calculations is the radial volume fraction profile of each molecule of type i, $\varphi_i(r)$.

From the radial distribution function it is straightforward to evaluate the excess number of molecules of type i in the small system

$$n_i^{\sigma} = \frac{\sum_r L(r)\left[\varphi_i(r) - \varphi_i^{b}\right]}{N_i} \tag{2}$$

N_i being the number of segments of species i. For example, when i refers to the surfactant species, $n_{surf}^{\sigma} = g$, that is the aggregation number of surfactants in the (reverse) micelle.

The relation between the bulk volume fraction φ_i^{b} and the molar concentration C_i of a species i is given by

$$C_i = \frac{\varphi_i^{b}}{N_a a^3 N_i} \tag{3}$$

a the size of one lattice site and N_a Avogadro's number.

Once the density and segment potential profiles are found in a self-consistent manner, the free energy follows and from that all other thermodynamic potentials. More specifically, we can evaluate the grand potential Ω_s as a function of the volume fraction and segment potential profiles.[10] The lower index s is added to indicate that we deal with a translationally restricted grand potential which differs from the overall grand potential by an entropic contribution. For dilute solutions of micelles we can estimate the ignored translational entropy of the micelle by $S_{trans} = -k_B \ln \phi_m$ where the volume fraction of micelles is found by $\phi_m = V_m/V_s$, with V_s the total volume of the system available per micelle and V_m the volume of a single micelle (which can be approximated by $g \times N_{surf}$). k_BT has its usual meaning. Then we have as a condition:

$$\Omega = \Omega_s - TS_{trans} = \Omega_s + k_BT \ln \frac{V_m}{V_s} = 0 \tag{4}$$

from this equation we see that $\Omega_s > 0$ as $k_BT \ln \frac{V_m}{V_s}$ is always negative. In our calculations we generate micelles with various aggregation numbers g yielding the function $\Omega_s(g)$. It can be shown that $-\partial\Omega_s/\partial g$ is inversely related to fluctuations in the micelle size. In other words, the stronger $\Omega_s(g)$ depends on the aggregation number, the more narrow is the size distribution of the reverse micelles. As negative size distributions cannot exist, for thermodynamic stability it is required that

$$\partial\Omega_s/\partial g < 0 \tag{5}$$

Spherical micelles are typically small so the translational entropy plays a significant role. For planar bilayers, on the other hand, this is not the case; we typically consider the cross-section of the bilayer only and normalise all properties by the area of the bilayer. Although the overall bilayer has some translational entropy per unit area the entropy can safely be ignored. In this case the grand potential can be identified by the membrane tension, and thus $\Omega = \Omega_s = 0$ or, in other words, the membrane tension of equilibrated bilayers is zero.

For a macroscopic planar interface, such as the water–vapour interface, the interfacial tension (γ) is of course finite. Since we consider only the properties across the interface, we normalise all quantities by the area of the interface.

Hence, the grand potential (Ω) is directly related to the interfacial tension γ as

$$\gamma = \frac{\Omega k_B T}{a^2} \tag{6}$$

this quantity is used below to evaluate the surface tension of the water–vapour interface as a function of the surfactant concentration.

7 The relation between adsorption and wetting

For obvious reasons our interest is drawn to the adsorption behaviour of CO_2 at the water–vapour interface, and how this adsorption is affected by the presence of surfactants. We already showed[10] that the adsorption isotherm of CO_2 on the water–vapour interface is a monotonically increasing function of the chemical potential of CO_2. The adsorbed amount Γ_{CO_2} (specified below) diverges as the chemical potential approaches the binodal value. The interpretation of this finding is that CO_2 completely wets the water–vapour interface.

Below we generate again a planar W–V interface and compute an adsorption isotherm $\Gamma_{CO_2}(\mu_{CO_2})$ but now in the presence of a surfactant. To find the isotherm we increased the amount of CO_2 in the system at a fixed volume fraction of surfactants in the bulk of the water phase. Unlike in the absence of a surfactant, it turned out that it was possible to find conditions for which the isotherm crossed the binodal condition $\mu_{CO_2} = \mu^{\#}_{CO_2}$ at a finite adsorbed amount, $\Gamma_{CO_2} = \Gamma^{\#}_{CO_2}$. Only when much more CO_2 was forced to be in the interface, the chemical potential relaxed to the bulk binodal value. Such isotherms are typical for cases where CO_2 does not wet the water–vapour interface completely. We say that such a surface is partially wet by CO_2. Hence, the surfactant induces a wetting (phase) transition.

It is well-known that wetting transitions can be either first or second order. The distinction between the two can easily be made by recording $\Gamma^{\#}_{CO_2}$ as a function of the control parameter, that is by recording $\Gamma^{\#}_{CO_2}(\varphi^{b}_{surf})$, where φ^{b}_{surf} is the bulk concentration of the surfactant (in the water phase). In the case where the adsorbed amount (at coexistence) $\Gamma^{\#}_{CO_2}(\varphi^{b}_{surf})$ smoothly increases and diverges at the wetting transition, this transition is second order.[18] If, at the wetting transition, this quantity diverges jump-like we have a first-order transition case.[18]

From the above it is clear that we need to evaluate Γ_{CO_2}. By choosing the phase rich in water as the bulk, we can evaluate the excess amount of each component θ^{σ}_i from:

$$\theta^{\sigma}_i = \sum_{z=1}^{M} \left(\varphi_i(z) - \varphi^{b}_i\right) \tag{7}$$

The excess number of molecules n^{σ}_i is then computed by

$$n^{\sigma}_i = \frac{\theta^{\sigma}_i}{N_i} \tag{8}$$

In order to define a surface excess, we need to choose a Gibbs reference plane, z^{Gibbs}. This is taken with respect to water,

$$z^{Gibbs} = \frac{\theta^{\sigma}_W}{\varphi_W(1) - \varphi_W(M)} \tag{9}$$

where $\varphi_W(1)$ is the volume fraction of water in the vapour phase and $\varphi_W(M)$ is the volume fraction of water in the water rich phase. Now the Gibbs excess of each component is given by

$$\Gamma_i = \frac{\theta^{\sigma}_i - z^{Gibbs}(\varphi_i(1) - \varphi_i(M))}{N_i} \tag{10}$$

8 Results and discussion

8.1 The water–liquid CO_2 interface

The experimentally determined water–liquid CO_2 interfacial tension (IFT) as a function of time, for different bulk concentrations (between 0.01 and 1.2% v/v) of Igepal CA520 in CO_2, is depicted in Fig. 2a. The measurements were continued upto 200 s. The temperature and pressure ranges are selected based on the conditions used in liquid CO_2 dry-cleaning,[4] which are $\sim$50 bar (*i.e.* $P/P_{sat} \approx 1.2$) and 283 K.

The densities of the CO_2 rich and CO_2 saturated water phases at the experimental pressures and temperatures were calculated using the equation of state of Span and Wagner[19]

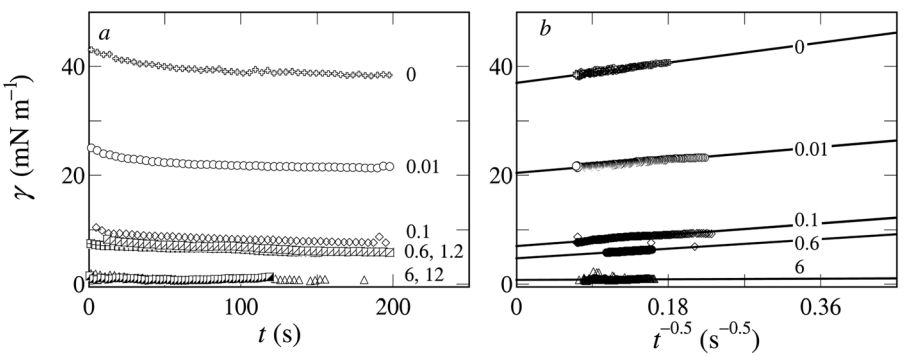

Fig. 2 (a) Dynamic interfacial tension between water and liquid CO_2 at 50 bar and 283 K for different surfactant concentrations in bulk liquid CO_2 as indicated (in (v/v)%). (b) The same IFT data plotted as a function of $t^{-0.5}$. The IFT data points are extrapolated to $t \to \infty$.

and eqn (3) and (4) in ref. 20. Further details can be found in ref. 10 and the references therein.

The water–CO_2 IFT clearly depends on the bulk concentration of the surfactant in liquid CO_2: the higher the concentration, the lower is the interfacial tension. This is the expected behaviour.

To obtain the equilibrium interfacial tension (γ_{eq}) corresponding to $t \rightarrow \infty$, we re-plotted the data (γ_t) of Fig. 2a against $t^{-0.5}$ and extrapolated to zero (Fig. 2b) following the well-known Ward and Tordai long-time approximation[21] as given by

$$\gamma_t = \gamma_{eq} + k\left(\frac{1}{\pi D t}\right)^{0.5} \quad (11)$$

In eqn (11), k is an experimental constant and D is the diffusion co-efficient of the surfactant in liquid CO_2. The intercepts obtained on the y-axis in Fig. 2b correspond to the equilibrium IFT data (γ_{eq}) for each bulk concentration. Although the interfacial tensions were measured for six different bulk concentrations, for clarity, only four surfactant concentrations are shown.

The γ_{eq} values obtained from Fig. 2b are plotted against the natural logarithm of the bulk concentration ($\ln C$) in Fig. 3a. We notice a CMC like behaviour, *i.e.* a change in the slope of γ_{eq} *versus* $\ln C$ beyond a concentration of $\sim$50 mM. We take this value as the critical reverse micellar concentration (CRMC) of Igepal CA520 in liquid CO_2.

The IFT–$\ln C$ curve obtained from self-consistent field modelling is presented in Fig. 3b. The calculations were done at P/P_{sat} = 1.2 and T = 283 K. In our model the value of P_{sat} is $\sim$110 bar[10] at 283 K.

The match between the experiment and the model is reasonable, keeping in mind that no *a posteriori* parameter fitting was attempted to match these two values. According to the model, the CRMC appears at $\sim$40 mM, as indicated in Fig. 3b while the experimentally measured reverse CMC was $\sim$50 mM (Fig. 3a).

The theoretical IFT–$\ln C$ curve does not display a CMC like cusp. This was expected as the experimental "cusp" is in fact an experimental "artefact". In the IFT calculation involving the water–CO_2 interface, the model assumes the surfactant chemical potential to simply increase; it does not take into account the self-assembly process taking place in the bulk and the presence of micelles must be inferred from complementary calculations; we discuss this in Section 8.3.

Next we looked at the adsorption of the surfactant at the water–CO_2 interface with increasing φ^b_{surf} in the water phase (Fig. 4). Fig. 4a and b correspond to a φ^b_{surf} of 10^{-8} and 10^{-6}, respectively. We clearly see an accumulation of surfactant at the water–liquid CO_2 interface. This excess surfactant at the interface lowers the water–CO_2 interfacial tension as found experimentally (Fig. 2). The surface excess increases with increasing bulk concentration. Moreover, we see that the hydrophilic head

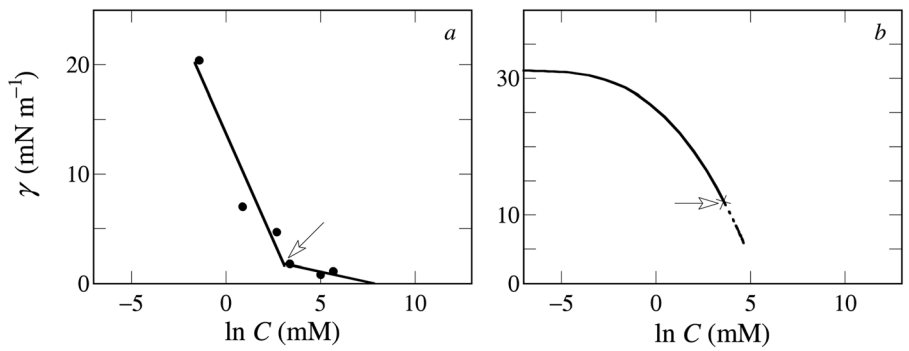

Fig. 3 (a) Equilibrium water–liquid CO_2 interfacial tension as a function of $\ln C$, the bulk concentration of surfactants in liquid CO_2 at 50 bar and 283 K. The experimental reverse micellar concentration of $\sim$50 mM is indicated. The two solid lines are linear fits of the experimental data points (b) water–liquid CO_2 IFT calculated from SF-SCF theory (at P/P_{sat} = 1.2). The theoretical reverse CMC is $\sim$40 mM and indicated in the figure.

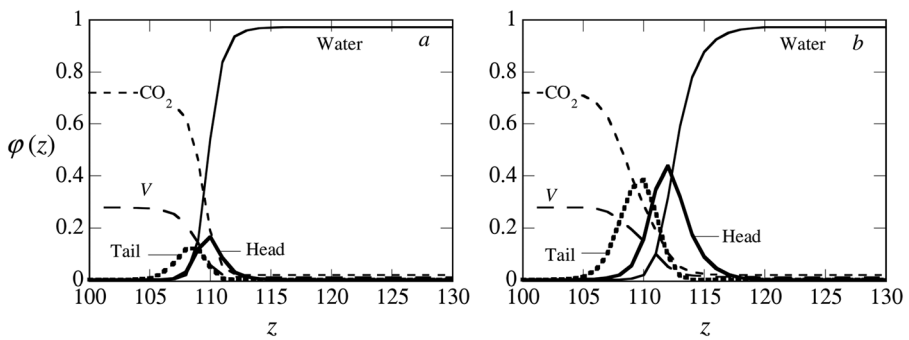

Fig. 4 SCF volume fraction profiles of various molecular species at the water–liquid CO_2 interface for a φ^b_{surf} of (a) 1×10^{-8} and (b) 1×10^{-6} in the water phase. The bulk CO_2 and water phases are situated at the left and the right side of the figures, respectively. The layer numbers z are arbitrary. P/P_{sat} = 1.2 and T = 283 K.

and the hydrophobic tail groups are disposed towards the water and the CO_2 phases, respectively. At the water–CO_2 interface we also notice an accumulation of the free volume, that is, a reduction in density.

8.2 Wetting transitions

In the previous results we focussed on the interface between water and CO_2. Such interfaces naturally develop when the pressure increases to values beyond saturation, so that liquid CO_2 is present in macroscopic amounts. However, at lower amounts of added CO_2 we have a water–vapour interface. We saw before that with increasing CO_2 concentration, liquid CO_2 appears at the water–vapour interface, or equivalently that the water–vapour interface is wet by liquid CO_2.[10]

We now consider what happens in the presence of the surfactant. As already explained, this involves the construction of adsorption isotherms of CO_2 at the W–V interface at a fixed concentration of the surfactant in the bulk; in this context the bulk is the water-rich phase. The Gibbs excess of CO_2 (Γ_{CO_2}) is given as a function of the chemical potential of CO_2 in Fig. 5a. The surfactant concentration in water (φ^b_{surf}) in this case is fixed at 5×10^{-7}. For comparison, we reproduce the result for $\varphi^b_{surf} = 0$ in Fig. 5b. From the shape of the adsorption isotherm in Fig. 5a, namely with an intersection of the line $\Delta\mu_{CO_2} = 0$ (saturation), we conclude that for this surfactant concentration the water–vapour interface is partially wet by CO_2. This implies that experimentally one expects the CO_2-phase to appear as a drop with a finite contact angle at the water–vapour interface.[22] The adsorbed amount, when the isotherm first crosses the coexistence condition, $\Gamma^{\#}_{CO_2}$, is finite.

Following this observation, we studied the surface phase diagram presented in Fig. 6. In this figure we plotted the Gibbs excess (the excess surface density) of CO_2 at the binodal (*i.e.* at co-existence), denoted by $\Gamma^{\#}_{CO_2}$ as a function of φ^b_{surf}, which appears to be a control parameter to tune the wetting behaviour.

Without any surfactant or at extremely low surfactant concentration ($\varphi^b_{surf} < 10^{-7}$), liquid CO_2 is present as a macroscopic thick film at the W–V interface. As the surfactant concentration in the bulk increases, $\Gamma^{\#}_{CO_2}$ becomes finite and

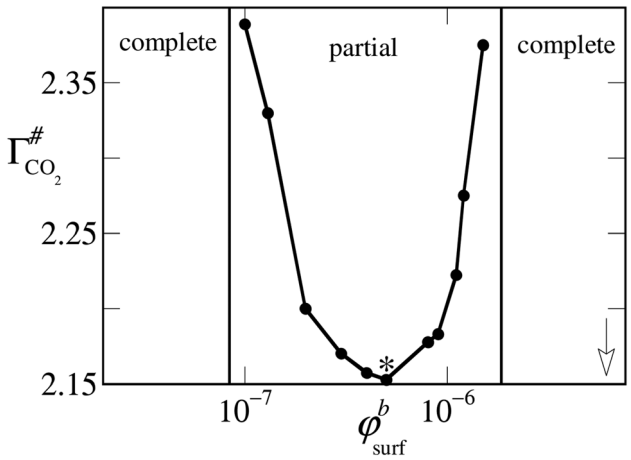

Fig. 6 Gibbs excess of CO_2 at the water–vapour interface when the isotherms cross the bulk coexistence value for the first time, $\Gamma^{\#}_{CO_2}$, as a function of the surfactant concentration in water. For all surfactant concentrations $\Gamma^{\#}_{CO_2}$ was finite and thus we have partial wetting. The two vertical lines indicate estimates for the lower and the upper bounds of the surfactant concentrations at which $\Gamma^{\#}_{CO_2}$ diverges, that is where the two wetting transitions occurred. The arrow indicated the surfactant concentration in the water phase at which the first reverse micelles appear in the CO_2 phase. The density profile of the point indicated by the * is given in Fig. 7.

a phase transition takes place from complete wetting to partial wetting. Upon further increase of the surfactant concentration, $\Gamma^{\#}_{CO_2}$ goes through a minimum and increases again to a second divergence corresponding to a second wetting transition.

In summary, Fig. 6 illustrates that there is re-entrant wetting behaviour: a window of surfactant concentrations for which the adsorbed amount of CO_2 remains finite and thus for which the water–vapour interface is not wet by CO_2. It was never observed that $\Gamma^{\#}_{CO_2}(\varphi^b_{surf})$ diverges jump-like when the wetting conditions are approached; this indicates that both transitions from partially wet to complete wet are most likely continuous, that is, they are of second order type. This is not too surprising because the CO_2–vapour system is relatively close to its critical point. Wetting transitions near critical points tend to be of second order type.[23]

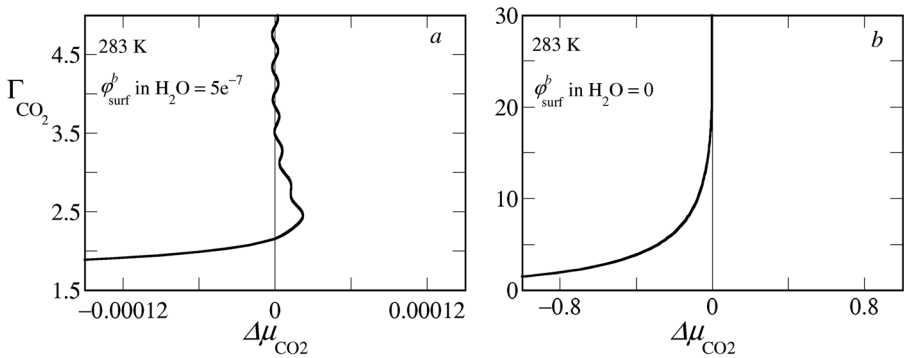

Fig. 5 Gibbs excess of CO_2 at the water–vapour interface as a function of $\Delta\mu_{CO_2} = \mu_{CO_2} - \mu^{\#}_{CO_2}$, where $\mu^{\#}$ is the chemical potential at coexistence, that is, at the binodal (a) in the presence of a volume fraction of 5×10^{-7} surfactant in the water phase and (b) in the absence of the surfactant. The adsorption isotherm in (a) indicates that the W–V interface is partially wet by CO_2, whereas in the case of (b) CO_2 completely wets the W–V interface.

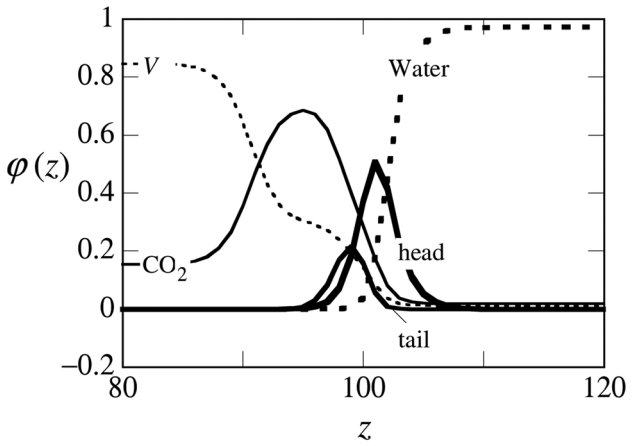

Fig. 7 Volume fraction profile of various molecular species at the three-phase co-existence of W, V and liquid CO_2 for a φ^{b}_{surf} of 5×10^{-7} in the water phase. The profiles corresponding to the point in Fig. 6 indicated by the asterisk. The layer numbers (z) are arbitrary.

Density profiles of the various species in the co-existence region at which $\Gamma^{\#}_{CO_2}$ is minimum are shown in Fig. 7. The profiles show that both CO_2 and the surfactant are present in excess at the W–V interface. The association of a finite amount of CO_2 with the surfactant layer is in line with the partial wetting of the W–V interface by CO_2, as explained above. We further notice that the surfactant head and tail groups reside in the water-rich and CO_2-rich phases, respectively. Moreover, the density of the CO_2 layer at the interface does not reach the bulk value, but is associated with a high V content. Hence, a shoulder is found in the V profile.

The re-entrant wetting can be rationalised based on the following argument: without any surfactant a thick layer of CO_2 spreads at the W–V interface as shown in Fig. 8a. This is in line with the critical point wetting as explained above. At low φ^{b}_{surf} when the interface is starved of surfactant monomers, CO_2 associates with the surfactant to form a less polar complex. This complex does not wet the W–V interface (Fig. 8b). CO_2 prefers to remain associated with the surfactant-rich islands.

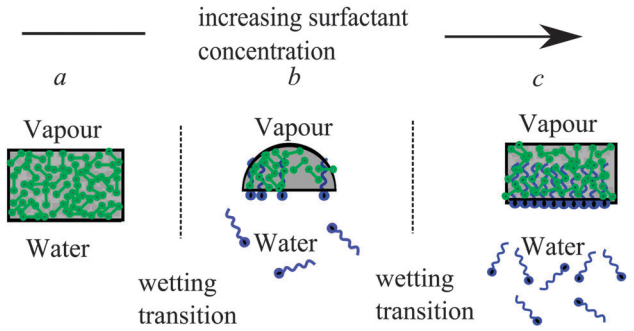

Fig. 8 Schematics of re-entrant wetting of CO_2 at the water–vapour interface. (a) A macroscopically thick CO_2 layer at the W–V interface without any surfactant (b) a drop of CO_2 at the W–V interface at a low concentration of surfactants and (c) re-appearance of a macroscopically thick layer of CO_2 upon further increase of surfactant concentration.

At higher φ^{b}_{surf}, the W–V interface has a fully developed monolayer of surfactants spreading at the interface, which helps CO_2 to spread at the interface as well. This scenario is depicted in Fig. 8c.

8.3 Self-assembly in bulk

Above we have discussed the calculations showing the effect of surfactant concentration on the water–CO_2 interfacial tension and wetting of the water–vapour interface by CO_2. In these calculations we used the surfactant concentration (in the water-phase) as the control parameter. Until now we assumed that this concentration could be imposed arbitrarily. We realize that this is possibly flawed, because of the possibility that association colloids are formed in either the water or the CO_2-rich phases or even both. The occurrence of such phenomena puts an upper limit to the (free) surfactant concentrations that can exist in the (water) phase. In the following sections we study the formation of surfactant mesophases in both bulk liquid CO_2 (reverse micelles) and water (bilayers) phases individually.

8.3.1 Reverse micelles in liquid CO_2. For any micellization to occur there must be a driving force and a stopping mechanism in order to have stable micelles. This holds true for both common and reverse micelles. The moieties that form the core of the micelles necessarily provide the driving force, and the moieties that end up in the corona of the micelles give the stopping force. The energy gain of the surfactant heads, which escape from the CO_2-rich phase, drives the assembly. Water co-assembles in the core, so the assembly is mediated by water. The loss in translational entropy of the chains goes against the micellization, and the hydrocarbon tails that want to remain solvated by CO_2 provide the stopping mechanism.

The grand potential (Ω_s) of a spherical micelle in the phase rich in CO_2 is plotted as a function of the surfactant aggregation number g (refer eqn (2)) in Fig. 9a in the phase rich in CO_2. The bulk volume fractions of water and free volume in the CO_2 rich phase correspond in this case to the three-phase co-existence conditions ($P = P_{sat}$).

Micelles in this phase are referred to as reverse micelles for obvious reasons. From Fig. 9a we notice that Ω_s becomes more positive with an increasing aggregation number and then goes through a maximum. As argued already, below the maximum (represented by the dashed part of the curve in Fig. 9a), the micelles are not thermodynamically stable.[24] Micelles for which $\partial\Omega_s/\partial g < 0$ are thermodynamically stable. The smallest micelles that are stable (corresponding to the maximum) may be identified as the micelles at the theoretical (reverse) CMC.

The equilibrium bulk concentration of the surfactant as a function of the number of surfactant molecules in the micelles is presented in Fig. 9b. The equilibrium concentration goes through a minimum at the same aggregation number where Ω_s shows a maximum. The value of φ^{b}_{surf} corresponding to the minimum can be identified as the reverse CMC and is found to be $\sim$33 mM (indicated by the asterisk). The relevant part of Fig. 9b (the solid curve) shows that with increasing size of the micelles the chemical potential increases slowly. We discuss

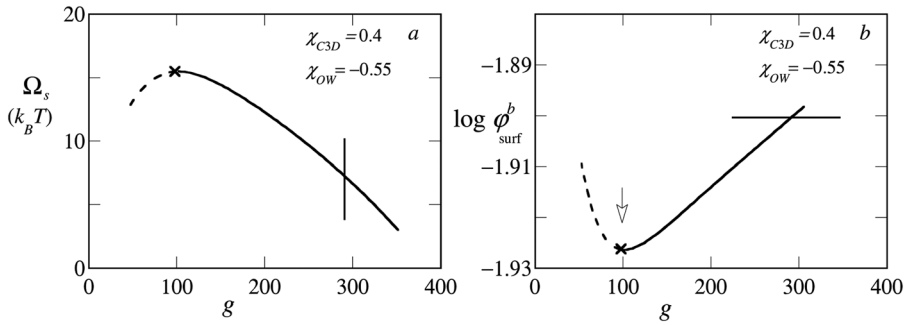

Fig. 9 (a) The grand potential Ω_s as a function of the surfactant aggregation number (g) for a spherical micelle with its center pinned to the center of the spherical coordinate system. (b) Corresponding $\log \varphi^{b}_{surf}$ as a function of the aggregation number g. The bulk volume fraction of water and free volume were taken to be consistent with three-phase co-existence conditions. The asterisks in (a) and (b) indicated the appearance of the first stable reverse micelles. The dashed regions of the curves indicated thermodynamically unstable reverse micelles. In panel (b) the horizontal line is drawn at the chemical potential above which surfactant bilayers appear in the water phase. In panel (a) the corresponding limit in the aggregation number g is indicated by the vertical line.

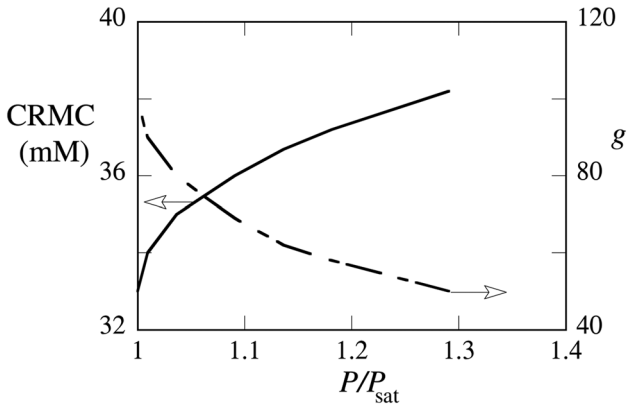

Fig. 10 SCF predictions for the reverse micellar concentration (left ordinate, solid curve) and the aggregation number (right ordinate, dashed curve) as a function of (reduced) pressure P/P_{sat}.

below that there is a limit to this increase of the chemical potential, as surfactant bilayers may form in the water phase.

We also consider the effect of pressure (beyond P_{sat}) on self-assembly in CO_2. Pressure is varied by varying the volume fraction of the free volume in CO_2. The reverse micelles become smaller and the critical reverse micellar concentration (CRMC) shifts to higher concentration with increasing pressure (Fig. 10). Apparently, liquid CO_2 becomes a better solvent for the surfactant with increasing pressure and the stopping mechanism for reverse micellization becomes stronger due to better solvation of the surfactant tails, leading to smaller reverse micelles and a higher CRMC. The theoretical CRMC at P/P_{sat} = 1.2 and temperature T = 283 K is ~40 mM. For the purpose of interpreting interfacial tensions, this value is indicated by the arrow in Fig. 3b. The match between the experimentally determined CRMC (~50 mM, see Fig. 3a) and the theoretically calculated one was reasonable taking into account that our model has not been fine-tuned. This is an interesting moment to assess the effects of two of the key parameters, namely χ_{C3D} and χ_{OW}, on the thermodynamics of micellization. The first one controls the solubility of the alkyl chain end in CO_2: it mediates the stopping mechanism. The second term expresses the tendency to co-assemble water in the reverse micelle: the more negative this value, the more water is taken up in the micelles. For this assessment, we return to the case of three-phase coexistence (P/P_{sat} = 1). Results are shown in Fig. 11a and b.

In Fig. 11a it is seen that with increasing repulsion between the methyl groups in the tail segment and CO_2, *i.e.* with increasing χ_{C3D} and decreasing solvent quality, micelles with higher aggregation numbers are formed. This is seen by the shift of the maxima to higher aggregation numbers. Our interpretation is that the

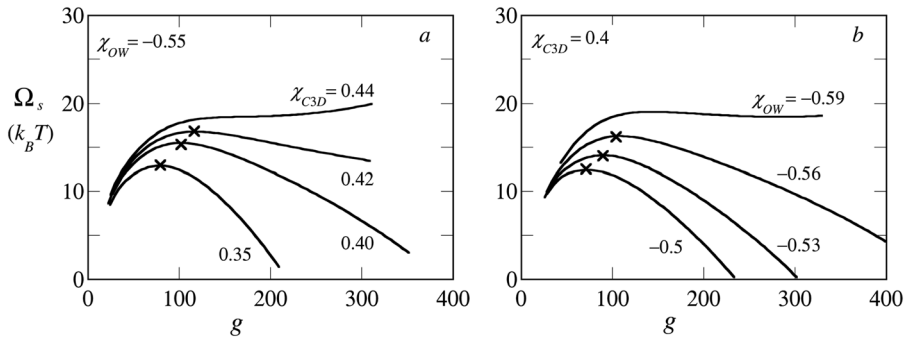

Fig. 11 Grand potential Ω_s as a function of aggregation number g for a spherical micelle (a) for various values of χ_{C3D} at fixed χ_{OW} = −0.55 and (b) for various values of χ_{OW} at fixed χ_{C3D} = 0.4. The volume fractions of water and free volume were taken to be consistent with three-phase coexistence *i.e.* at P/P_{sat} = 1.

stopping mechanism becomes weaker with increasing χ_{C3D}, the tail segments reduce their contacts with CO_2 by forming larger reverse micelles, and they repel each other less. Moreover, we notice that $\partial\Omega_s/\partial g$ becomes less negative with higher χ_{C3D}, indicating more polydisperse (wider size distribution) reverse micelles.[16] Beyond $\chi_{C3D} = 0.42$ stable reverse micelles cannot be formed as $\partial\Omega_s/\partial g$ is no longer negative. This sets the upper limit of χ_{C3D} for having spherical reverse micelles in the CO_2-rich phase. Favourable tail–CO_2 interactions (lower χ_{C3D}) result in reverse micelles with a lower aggregation number indicating a stronger stopping mechanism.

The effect of χ_{OW} can be seen from Fig. 11b. An increase in attraction between the oxygen of the surfactant and water increases the driving force for reverse micellisation. Hence, the more negative χ_{OW}, the larger reverse micelles are formed, as evident from the shift of the maxima to a higher aggregation number. Of course, with more driving force for self-assembly one should also provide a stronger stopping mechanism. In fact by fixing $\chi_{C3D} = 0.4$ the stopping force becomes gradually insufficient to limit the growth of the micelles. As a result we see a gradual growth of the micelle size distribution with more negative χ_{OW}-values, and beyond $\chi_{OW} = -0.56$ the spherical micelles lose stability ($\partial\Omega_s/\partial g$ is no longer negative). Hence, increasing attraction between water and the head group oxygen leads to reverse micelles with higher aggregation numbers, and eventually an insufficient stopping mechanism then leads to disappearance of spherical micelles.

Table 1 Flory–Huggins interaction parameters (χ) between various pairs of segments at 283 K. Here D is the monomer in CO_2, W is the monomer in water, V is the empty site, C is the CH_2 segment, C3 is the alkyl segment at the (branched) hydrocarbon end of the surfactant and O is the head group oxygen of the surfactant. We assume a $1/T$ dependence for these interaction parameters. The set of parameters has more rounded values for $T = 300$ K

χ	D	W	V	C	C3	O
D	0	1.65	1.65	0.99	0.4	1.66
W	1.65	0	3.87	0.99	1.55	−0.55
V	1.65	3.87	0	1.77	1.55	3.87
C	0.99	0.99	1.77	0	0.55	1.77
C3	0.4	1.55	1.55	0.55	0	2.21
O	1.66	−0.55	3.87	1.77	2.21	0

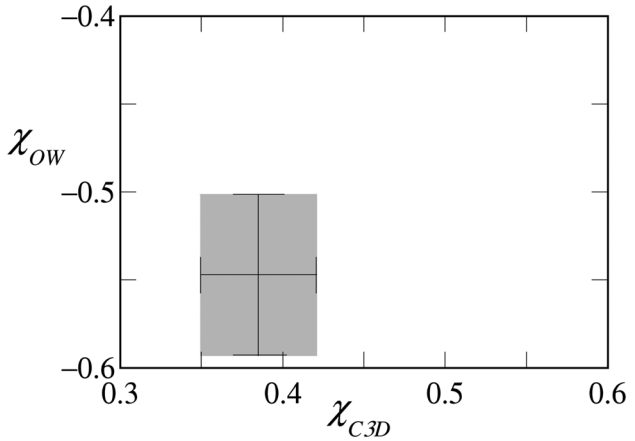

Fig. 12 The stability window (shaded area) for spherical reverse micelles with respect to two key interaction parameters, χ_{C3D} and χ_{OW} at $P/P_{sat} = 1$. The volume fractions of water and free volume were taken to be consistent with three-phase coexistence, *i.e.* at $P/P_{sat} = 1$.

Now that the window of stability of the spherical reverse micelles in the CO_2-rich phase (Fig. 12) has been identified, it is worth discussing the SCF prediction for the radial volume fraction distribution of the various segments in a typical reverse micelle having an aggregation number 150 (Fig. 13a). All interaction parameters have their default values (Table 1). The radial volume fraction profiles of a reverse micelle clearly prove the presence of significant amounts of water inside the core. In the corona the volume fraction of CO_2 is relatively high, which is consistent with the fact that the alkyl part of the surfactant is solvated by CO_2. In the corona some free volume is also present, imparting a reduced density to the tails.

8.3.2 Surfactant bilayers in the water phase. We saw that spherical reverse micelles can be thermodynamically stable, but that the parameter space with respect to χ_{OW} and χ_{C3D} is not particularly wide. In principle, we should also further analyse the stability of cylindrical or lamellar structures in the CO_2-rich phase. For the moment we skip such an analysis and only mention that the competing association colloid that is identified in this system is a bilayer structure (lamellar) that may form in the water-rich

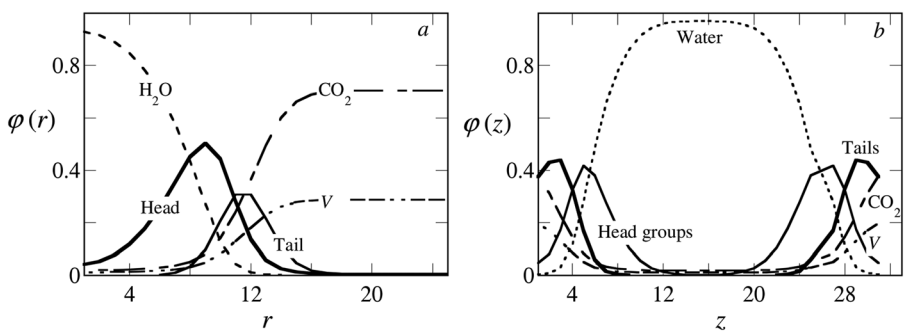

Fig. 13 Volume fraction distributions of various molecular species, (a) radial distribution for a spherical micelle in the CO_2 rich phase with $g = 150$ and (b) volume fraction distribution of molecular species for two halves of two tensionless bilayers situated at a center-to-center distance $d = 30$ in water. At the centre of both bilayers reflecting boundary conditions were applied implying an infinite array of bilayers. Both systems are at the three phase co-existence of water, V and CO_2 at 283 K. All parameters have the default values (Table 1).

phase, although we cannot fully exclude that non-spherical micelles may form at elevated surfactant concentrations.

Turning our attention to the water phase, we performed calculations in which the bulk volume fractions of CO_2 and free volume in water were fixed to the values corresponding to the three-phase co-existence condition and 283 K. Considering the molecular architecture of the surfactant we note a relatively bulky apolar moiety (the alkyl and the benzene ring) and a relatively short ethylene oxide head group. This suggests a packing parameter of order unity. Therefore it is natural to consider the relative stability of bilayer membranes in the water-rich phase.

To study bilayers we select a planar lattice and pin the bilayer with its symmetry-plane to the edge of the lattice where we impose reflecting boundary conditions. In such a way we are able to remove the translational entropy of the bilayer. Again we compute Ω_s, now as a function of the number of surfactants per unit area (g). We vary the number of surfactants in the bilayer until we find the condition that the bilayer is free of tension, that is when $\Omega_s = \gamma = 0$. We do not present the $\Omega(g)$ curve here. Instead, we directly discuss the structure of the bilayers found by this procedure. We notice that the chemical potential (*i.e.* $\log \varphi^{b}_{surf}$) associated with the reverse micelle formation in the CO_2-rich phase is lower than that associated with the formation of the bilayer in the water phase (-1.93 for the formation of reverse micelle *versus* -1.9 for the bilayer formation in water). Hence, the reverse micelles in the CO_2-rich phase come first. As the surfactant concentration in the CO_2-rich phase increases further, the aggregation number of the reverse micelles increases and the chemical potential starts rising (as indicated in Fig. 9b). This is not a favourable situation and the system can lower its free energy by forming bilayers in the water phase instead. In Fig. 9b this is indicated by a horizontal line at the chemical potential at which the bilayers form. The aggregation number of micelles is therefore limited to $g \approx 290$. Accordingly, a vertical line in Fig. 9a has been placed.

In Fig. 13b we present the volume fraction profiles of the molecular components in the tensionless bilayer. Here we choose to plot the distributions over two bilayers which are separated by a core-to-core distance $d = 30$ (in lattice units). As reflecting boundary conditions were applied between layers $z = 0$ and $z = 1$ and between layers $z = 30$ and $z = 31$, it suffices to give only the distributions of half the bilayers. In between the bilayers there is a (bulk) water phase. The volume fractions of the free volume and CO_2 in this water phase are fixed according to the three-phase co-existence conditions.

We see that the head groups are associated with a finite fraction of water, whereas the tails are well shielded from water. We also notice that there are finite amounts of free volume ($\varphi_z \sim 0.2$) and CO_2 ($\varphi_z \sim 0.4$) accumulated in the tail region of the bilayer, making the bilayers quite compressible. It is rather important for the stability of these bilayers that there is just a finite amount of these "solvents" in the core. An unlimited swelling of the bilayers with CO_2 (and/or V) will hinder the stability of these mesophases. Apparently there is a free energy barrier against the unbounded growth of the CO_2 and/or the free volume phase in the bilayers, even though the chemical potentials allow for the formation of such phases. The finding that the swelling of the bilayers remain finite is in some respect surprising. As one might expect, when a V-phase would form in the bilayer, the CO_2 layer should spontaneously develop as well and grow without bounds: this is because the wetting study proved the absence of a barrier in this case. However, the V-phase cannot form in the absence of sufficient CO_2. Apparently, as a result there existed a barrier against the growth of the phases inside the bilayers. By which exact mechanism this barrier is put in place by the surfactant molecules remains unexplained.

The colloidal stability of the bilayers is further investigated by studying the inter-bilayer interactions as a function of distance (Fig. 14). We follow the change in μ_{surf} for the tensionless bilayers as a function of an imposed core-to-core distance between two bilayers d. More specifically, we focus on $\Delta\mu(d)$, which is the difference in chemical potential of the surfactants when two bilayers are at a certain distance d and when they are far apart, *i.e.* $d = \infty$. Physically, with decreasing d we mimic an increase of the total surfactant concentration in the water phase.

In Fig. 14 interaction curves $\Delta\mu_{surf}$ are given for various values of the key interaction parameters χ_{C3D} and χ_{OW}. We observe that $\Delta\mu$ decreases with increasing d. Physically this means that the bilayers are repulsive. At large distances ($d/2 > 11$) we do not see any interaction between the bilayers, simply because the bilayers are not in contact with each other. The origin of the repulsion is not easily identified. Several phenomena occur simultaneously

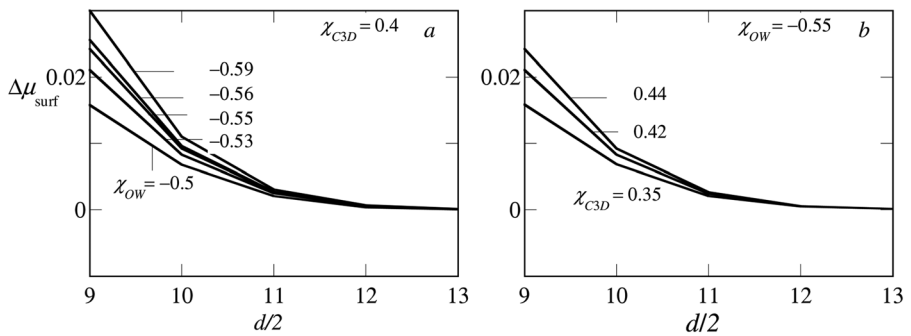

Fig. 14 Change in chemical potential ($\Delta\mu_{surf}$) as a function of (half) the core–core distance between two bilayers (a) for various χ_{OW} and fixed $\chi_{C3D} = 0.4$ and (b) for various χ_{C3D} at fixed $\chi_{OW} = -0.55$. The chemical potentials of CO_2 and free volume were chosen to represent three-phase coexistence ($P/P_{sat} = 1$).

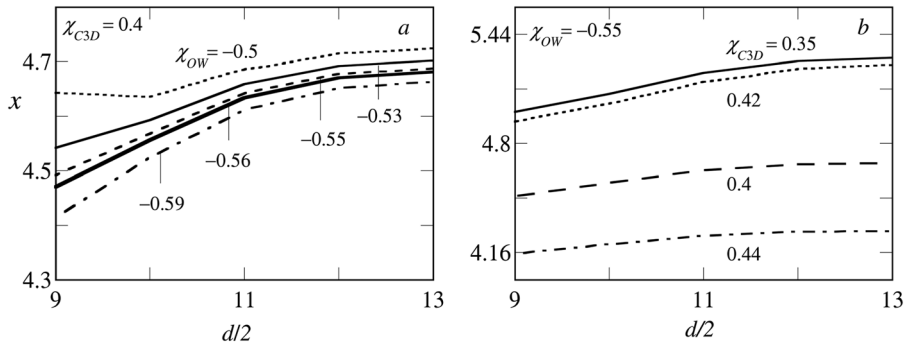

Fig. 15 Ratio x between the excess number of CO_2 molecules and the excess number of surfactant molecules in the bilayers as a function of compression for varying (a) χ_{OW} and (b) χ_{CD}. The volume fraction of water and free volume were taken to be consistent with three-phase coexistence (P/P_{sat} = 1).

upon compression of the bilayers. As the membranes remain free of tension, the area per surfactant molecule adjusts itself. This implies some deformation of the surfactant layer, that is, the corona may be compressed or the tails may be squeezed.

As can be seen in Fig. 14a, with increasing favourable interactions between O and W (more negative χ_{OW}), the repulsion between the bilayers increases. This was expected, as more favourable interactions between the head group oxygen and water mean more resistance towards compression, leading to higher repulsion and more stable bilayers.

Similar behaviour is noticed when the parameter χ_{C3D} is varied keeping constant χ_{OW} (Fig. 14b). The higher the χ_{C3D}, the stronger is the repulsion between the C3 and D segments, and the less CO_2 (and free volume) accumulates in the cores of the bilayers. Hence, it becomes more difficult to compress the bilayers. In this context, the molecular composition of the bilayers during compression is of interest. We consider the ratio between the number of CO_2 molecules and the number of surfactants in the bilayer, defined by the variable $x = \theta_{CO_2}N_{surf}/\theta_{surf}N_{CO_2}$. In Fig. 15a and b we report x as a function of (half) the inter-bilayer spacing for varying χ_{OW} and χ_{CD}, respectively. We see that as the bilayers are compressed, for both the cases (varying χ_{OW} and χ_{CD}) the value of x decreases. Hence, the repulsion is in part due to the loss of CO_2 *i.e.*, reduction of x. The number of surfactant molecules per unit area also decreases (not shown). This means that during compression the total membrane area increases. Nevertheless, the bilayer remains thermodynamically stable.

We further notice that the higher the attraction between the head group oxygen and W, the stronger is the decrease of x upon compression. This is because for more negative χ_{OW}, the increase of the excess surfactant molecules in the bilayers becomes energetically more favourable. Similarly, the penalty in energy to push out CO_2 molecules out of the bilayers becomes higher with increasing repulsion between the methyl groups of the tails and CO_2. The higher χ_{C3D}, the lower is the amount of CO_2 in the surfactant tail regions and the less compressible are the bilayers.

Above we noticed that the bilayers in the water phase are colloidal stable: they do not attract each other. In other words we do not see the formation of a lamellar phase. However, it must be mentioned that we do not account for attractive van der Waals interactions between bilayers. These interactions should be added to the pair potentials *a posteriori*.

8.4 Conclusion and outlook

We experimentally verified the interfacial activity of a branched hydrocarbon surfactant, Igepal CA520, at the water–CO_2 interface at 50 bar and 283 K. The IFT between water and liquid CO_2 decreases with increasing surfactant concentration in the bulk CO_2 phase. The experimental IFT–ln C curve shows a CMC like cusp and from this curve the onset of self-assembly in the bulk was found to be $\sim$50 mM. These measurements were complemented by SCF modelling. Although the model needs many parameters, which are still subject to further optimisation, it is satisfying to mention that the model semi-quantitatively predicted the correct CRMC of $\sim$40 mM. The modelling results also deepened our understanding behind the molecular processes of wetting, adsorption and self-assembly in these systems.

Using the surfactant concentration as the control parameter, we predict a pair of wetting transitions for the CO_2 phase at the water–vapour interface. Both in the absence of a surfactant and at high surfactant concentrations the water vapour interface is wet by CO_2. At intermediate surfactant concentrations, yet below the CRMC, the water–vapour interface is wet partially by CO_2. Intuitively we expected that this would affect the stability of the bilayers in the water phase, but this is not the case. Both wetting transitions, that is the wetting transition from complete to partial at the re-entrant wetting transition, are of the second order type. We are not too surprised by this, because the system is close to the critical point. Again, both wetting transitions occur below the critical reverse micellar concentration and therefore also below the bulk volume fraction of the surfactant that is in equilibrium with the surfactant bilayers in the water phase.

The reverse micelles in liquid CO_2 are stable for a narrow range of χ_{OW} and χ_{C3D} at P/P_{sat} = 1. With increasing pressure the stopping force for micellisation becomes stronger. Hence, with increasing pressure the parameter window for the micellisation widens a bit. Nevertheless we found that the thermodynamic stability of the micelles is easily lost. This might explain in part why in practice the search for proper surfactants in liquid CO_2 systems has been so frustrating. Our results may pave the way to study the effects of various structural units, such as the length of

the EO groups, the degree of branching and the number of C3 or C in the surfactant tail region, on the process of reverse micellization. The understanding emerging from these studies would provide guidelines for the design of surfactants for liquid CO_2.

We used the self-consistent field theory to compare the self-assemblies in the bulk CO_2 and in water. More specifically, we determined the chemical potential needed for the formation of reverse micelles in the CO_2 rich phase and bilayers in the water phase. From this it follows that with increasing surfactant concentration first reverse micelles form in CO_2 followed by bilayers in water. These findings should be verified by X-ray or neutron scattering studies. Preliminary X-ray scattering data in a ternary system of Igepal CA520, liquid CO_2 and water show the signature of surfactant reverse micelles. These results will be published in a follow up article.

Appendix

SCF formalism for planar geometry

The water–liquid CO_2 and water–vapour interfaces as well as the bilayer formation in the water phase have been modelled using planar lattices. Calculation of the volume fraction of segments s of chain i containing N segments follows from the chain segment weighting factors, $G_i(z,s|1;N)$. The notation implies that for a chain there are two complementary walks that begin from opposite ends, one from segment 1 and the second from the other end, N. Both these walks terminate at s, which is at coordinate z. The composition law combines the two walks consisting of $s-1$ and $N-s$ steps, respectively.[15,25,26]

$$G_i(z,s|1;N) = \frac{G_i(z,s|1)G_i(z,s|N)}{G_i(z,s)} \tag{12}$$

The term in the denominator, which is the statistical weight of a free segment s at coordinate z, is included in both the walks and corrects for double counting. The summation over all segments $s = 1, \ldots, N_i$ of all these distribution functions results in the volume fraction of molecule i in layer z and is given by,

$$\varphi_i(z) = C_i \sum_{s=1}^{N_i} \frac{G_i(z,s|1)G_i(z,s|N)}{G_i(z,s)} \tag{13}$$

C_i is a normalization factor and is given by,

$$C_i = \frac{\theta_i}{N_i G_i(N|1)} \tag{14}$$

where the single chain partition function

$$G_i(N|1) = \sum_z G_i(z,N|1) \tag{15}$$

and

$$\theta_i = \sum_i \varphi(z) \tag{16}$$

The end point distribution functions are calculated using a propagator scheme. We gave the propagator formalism of small molecules such as CO_2 and water in our previous publication[10] and in this section we deal with the surfactant, which is a chain like molecule.

The free segment distribution function for segments at layer z is $G_i(z,s)$. This quantity is related to the free segment distribution function of a segment type X at co-ordinate z, $G_X(z)$, while segment s is of type X. Mathematically,

$$G_i(z,s) = \sum_X \delta_{i,s}^X G_X(z) \tag{17}$$

Here X represents the segment types (C3 or C or O) and the summation is over all segment types. $\delta_{i,s}^X$ is unity if the segment s of molecule i is of type X and zero for all other types of segments. The forward and backward propagators read

$$\begin{aligned} G_i(z,s|1) &= G_i(z,s) \sum_{z'=z-1,z,z+1} \lambda_{z-z'} G_i(z',s-1|1) \\ &= G_i(z,s)\langle G_i(z,s-1|1)\rangle \end{aligned} \tag{18}$$

$$\begin{aligned} G_i(z,s|N) &= G_i(z,s) \sum_{z'=z-1,z,z+1} \lambda_{z-z'} G_i(z',s+1|N) \\ &= G_i(z,s)\langle G_i(z,s+1|N)\rangle \end{aligned} \tag{19}$$

The angular parentheses stand for an average over three layers and $\lambda_{z-z'}$ is the *a priori* step probability to go from a layer z' to z. The propagators are started realizing that $G_i(z,1|1) = G_i(z,1)$ and $G_i(z,N|N) = G_i(z,N)$.

The segmental weighting factor for segment type X has already been discussed at length in our previous publication[10] and is given by

$$G_X(z) = \exp\left(\frac{-u_X(z)}{k_B T}\right) \tag{20}$$

where,

$$u_X(z) = \alpha(z) + K_B T \sum_Y \chi_{XY}\left(\langle \varphi_Y(z) - \varphi_Y^b \rangle\right) \tag{21}$$

$G_X(z)$ is the probability of finding a free segment X in layer z relative to that of finding it in a layer in the homogeneous bulk solution.[10]

The first term in eqn (21) is the Lagrange parameter, an entropic term, which represents the excluded volume interactions with respect to the bulk solution and is independent of the segment type; $\alpha(z)$ is an adjustable parameter, which ensures the incompressibility condition $\sum_i \varphi_i = 1$ in each layer. The second term is an enthalpic term and arises from interactions between segments X and Y; $\langle \varphi_Y(z)\rangle$ is the site average volume fraction of Y in layer z and contains contact contributions from neighbours in layer $z-1$, z and $z+1$. The site volume fractions, which are an average over three consecutive layers are given by,

$$\langle \varphi_X(z)\rangle = \lambda_{-1}\varphi_X(z-1) + \lambda_0\varphi_X(z) + \lambda_1\varphi_X(z+1) \tag{22}$$

where $\lambda_{z'-z}$ is the fraction of contacts of a site in layer z with sites in layer z' with z' equal to $z-1$, z or $z+1$. The first term inside the summation in eqn (21) is the Flory–Huggins interaction parameter (χ) and takes into account the short range attractive and repulsive interactions between molecules at

segment levels. The final term in eqn (21) is the excess volume fraction of segment Y in layer z (averaged over three consecutive layers) with respect to the bulk volume fraction of Y, φ_Y^b.

We have so far given the expressions for linear molecules having different segments in their backbone. The surfactant molecule that we used in our model contains C3 branching and also the benzene ring was represented as a branched moiety. The propagators for this type of molecule can be found in ref. 27. In the next section we delineated the differences between the flat and spherical lattices.

Details of spherical lattices

The formation of spherical self-assembled objects was studied by placing the molecules inside a spherical lattice and the SCF machinery was adjusted accordingly. In a spherical lattice we specified $r = 1, \ldots, r_M$ layers, the first layer being at the centre of the lattice. At the other end, *i.e.* right after layer r_M, a mirror like boundary condition was imposed. Unlike in the planar lattice, the number of lattice sites, $L(r)$, is a non-trivial function of the coordinate r. More specifically for spherical geometry $L(r) = V(r) - V(r-1)$, where $V(r) = \frac{4}{3}\pi r^3$ is the volume of the layer r. The key difference with the planar lattice is that the number of lattice sites is different in each layer and hence λ_{-1}, λ_0 and λ_1 are functions of the radial coordinate r. The ''inversion symmetry'' dictates

$$\lambda_{-1}(r)L(r) = \lambda_1(r-1)L(r-1) \tag{23}$$

As $L(r)$ is an increasing function of r, the transition probabilities λ also become r-dependent. The expressions are given below.

$$\lambda_1(r) = \lambda_1^b \frac{S(r)}{L(r)} \tag{24}$$

and

$$\lambda_{-1}(r) = \lambda_{-1}^b \frac{S(r-1)}{L(r)} \tag{25}$$

and

$$\lambda_0(r) = 1 - \lambda_1(r) - \lambda_{-1}(r) \tag{26}$$

The λ_1^b and λ_{-1}^b in the above equations are the correcting factors pertaining to the equivalent planar lattice and $S(r) = 4\pi r^2$ is the contact area.

The total amount of molecule i, θ_i, is related to the volume fraction of molecule i in layer r by

$$\theta_i = \sum_i L(r)\varphi_i(r) \tag{27}$$

and the single chain partition function, $G_i(N|1)$, reads in this geometry as:

$$G_i(N|1) = \sum_i L(r)G_i(r, N|1) \tag{28}$$

The notations have the same meaning as those explained for the planar lattice case.

References

1 R. Nagarajan and E. Ruckenstein, *Langmuir*, 2000, **16**, 6400–6415.
2 R. Nagarajan and E. Ruckenstein, *Langmuir*, 1991, **7**, 2934–2969.
3 W. Ryoo, S. E. Webber and K. P. Johnston, *Ind. Eng. Chem. Res.*, 2003, **42**, 6348–6358.
4 S. Banerjee, S. Sutanto, J. M. Kleijn and M. A. Cohen Stuart, *Colloids Surf., A: Physicochemical and Engineering Aspects*, 2012, **415**, 1–9.
5 R. G. Larson, L. E. Scriven and H. T. Davis, *J. Chem. Phys.*, 1985, **83**, 2411–2420.
6 M. Lísal, C. K. Hall, K. E. Gubbins and A. Z. Panagiotopoulos, *J. Chem. Phys.*, 2002, **116**, 1171–1184, DOI: 10.1063/1.1428347.
7 S. Salaniwal, S. T. Cui, P. T. Cummings and H. D. Cochran, *Langmuir*, 1999, **15**, 5188–5192.
8 S. Salaniwal, S. Cui, H. D. Cochran and P. T. Cummings, *Ind. Eng. Chem. Res.*, 2000, **39**, 4543–4554.
9 S. Salaniwal, S. T. Cui, H. D. Cochran and P. T. Cummings, *Langmuir*, 2001, **17**, 1773–1783.
10 S. Banerjee, E. Hassenklöver, J. M. Kleijn, M. A. Cohen Stuart and F. A. M. Leermakers, *J. Phys. Chem. B*, 2013, **117**, 8524–8535.
11 B. R. Postmus, F. A. M. Leermakers and M. A. Cohen Stuart, *Langmuir*, 2008, **24**, 3960–3969.
12 Y. Sutjiadi-Sia, P. Jaeger and R. Eggers, *J. Supercrit. Fluids*, 2008, **46**, 272–279.
13 A. Georgiadis, G. Maitland, J. P. M. Trusler and A. Bismarck, *J. Chem. Eng. Data*, 2010, **55**, 4168–4175.
14 P. Chiquet, J. Daridon, D. Broseta and S. Thibeau, *Energy Convers. Manage.*, 2007, **48**, 736–744.
15 O. A. Evers, J. M. H. M. Scheutjens and G. J. Fleer, *Macromolecules*, 1990, **23**, 5221–5233.
16 F. A. M. Leermakers and J. M. H. M. Scheutjens, *J. Colloid Interface Sci.*, 1990, **136**, 231–241.
17 M. J. Hollamby, K. Trickett, A. Mohamed, R. S. E. J. Eastoe and R. K. Heenan, *Langmuir*, 2009, **25**, 12909–12913.
18 M. Schick, *Liquids at Interfaces*, *Proc. Les Houches Session XLVIII*, 1988, **1990**, 416.
19 R. Span and W. Wagner, *J. Phys. Chem. Ref. Data*, 1996, **25**, 1509–1596.
20 A. Hebach, A. Oberhof and N. Dahmen, *J. Chem. Eng. Data*, 2004, **49**, 950–953.
21 P. Joos and V. B. Fainerman, *Dynamic Surface Phenomena*, VSP, Utrecht, 1999.
22 B. V. Derjaguin, N. V. Churaev and V. M. Muller, *Surface Forces*, Plenum Press, New York, 1960.
23 J. W. Cahn, *J. Chem. Phys.*, 1977, **66**, 3667–3672.
24 P. N. Hurter, J. M. H. M. Scheutjens and T. A. Hatton, *Macromolecules*, 1993, **26**, 5592–5601.
25 J. M. H. M. Scheutjens and G. J. Fleer, *J. Phys. Chem.*, 1979, **83**, 1619–1635.
26 O. A. Evers, J. M. H. M. Scheutjens and G. J. Fleer, *J. Chem. Soc., Faraday Trans.*, 1990, **86**, 1333–1340.
27 L. A. Meijer, F. A. M. Leermakers and J. Lyklema, *J. Chem. Phys.*, 1999, **110**, 6560–6579.

